Supercurrents Through Single-Walled Carbon Nanotubes

A. Yu. Kasumov,[1,2] R. Deblock,[1] M. Kociak,[1] B. Reulet,[1] H. Bouchiat,[1]* I. I. Khodos,[2] Yu. B. Gorbatov,[2] V. T. Volkov,[2] C. Journet,[3] M. Burghard[4]

Proximity-induced superconductivity in single-walled carbon nanotubes below 1 kelvin, both in a single tube 1 nanometer in diameter and in crystalline ropes containing about 100 nanotubes, was observed. The samples were suspended between two superconducting electrodes, permitting structural study in a transmission electron microscope. When the resistance of the nanotube junction is sufficiently low, it becomes superconducting and can carry high supercurrents. The temperature and magnetic field dependence of the critical current of such junctions exhibits unusual features related to their strong one-dimensional character.

Depending on diameter and helicity, single-walled carbon nanotubes (SWNTs) have, at most, two conducting channels (*1*) with minimum resistance in the absence of disorder predicted to be $h/4e^2 = 6.5$ kilohms. Electron-electron interactions in such systems are predicted to give rise to non-Fermi (Luttinger) liquid behavior at low temperature (*2*). From the magnetic field dependence of the tunneling conductance of an SWNT indicating strong spin correlations, it has been suggested that magnetic ordering could take place in SWNTs (*3*). Such electronic properties seem incompatible with the occurrence of superconductivity. We show that it is possible to create superconducting junctions with carbon nanotubes embedded between superconducting contacts. When the normal state resistance of the tube is sufficiently low, the sample exhibits a zero resistance low-temperature state and a high critical supercurrent.

A normal metal (N) in contact with a macroscopic superconductor (S) exhibits superconductivity on a characteristic length which is smaller than both the phase coherence length in the normal metal L_ϕ and the thermal length L_T (in a clean metal $L_T = \hbar v_f/k_B T$ and in a dirty metal $L_T = \sqrt{\hbar D/k_B T}$, where D is the electron diffusion coefficient). Both lengths, on the order of a few micrometers, can be much longer than the superconducting coherence length. The superconducting transition temperature T_c and the gap Δ in N can be on the order of their values in S if the resistance of the SN interface is sufficiently small. This proximity effect has been extensively studied in multilayered planar SN junctions (*4*) and more recently in lithographically fabricated micrometer-scale metallic wires made of normal noble metals between two macroscopic superconducting electrodes (*5, 6*). The maximum low-temperature value of the supercurrent (critical current) in such SNS junctions is $\pi\Delta/eR_N$, where R_N is the normal resistance of the junction (*7*). We show that the supercurrent sustained by a single nanotube exceeds this prediction by a large factor.

The SWNTs were prepared by an electrical arc method with cobalt as a catalyst (*8*), yielding single-walled tubes with diameters on the order of 1 nm. The tubes were usually assembled in ropes of about 100 parallel tubes, but individual tubes can also be obtained after purification (*9*). Isolation of an individual rope or tube and connection to electrical contacts were performed according to the procedure we previously used for multiwalled nanotubes (*10*). The resulting junctions had low-resistivity ohmic contacts between the tube and the metal electrodes (molten during the process), and could be characterized using transmission electron microscopy (Fig. 1) (*11*). The use of superconducting bilayer electrodes (Re/Au or Ta/Au) gives rise to the proximity effect. Rhenium or Ta ensures good adhesion to the substrate and promotes superconductivity of contacts; the immiscibility of the Re/Au and Ta/Au systems (both solid and liquid) and the very high melting temperature of Re and Ta prevents electrode damage during laser welding of the tubes to the top Au layer. Gold is an ideal solder for nanotubes because it neither reacts with carbon nor oxidizes.

The room temperature resistance, R_0, of such junctions varied considerably from sample to sample, typically between 0.100 and 100 kilohms. For ropes, when R_0 was on the order of or larger than 10 kilohms, a sharp divergence of the resistance was observed below $T = 50$ K, corroborating experimental results obtained by other groups (*12*). This low-temperature insulating behavior has been attributed to the helicity of the tubes or to the existence of defects such as heptagon-pentagon pairs. It has also been theoretically shown (*13*) that Van der Waals interaction between individual nanotubes in a rope can induce a band gap of about 0.1 eV, making a rope consisting of individually metallic tubes semiconducting. We found that it is also possible to obtain samples with resistance lower than 6.5 kilohms, indicating that a large fraction of the tubes participate in transport. This is the case for three samples, where the resistance decreases slightly with temperature between room temperature and 4.2 K (Fig. 2). So far, such low values of R_0 and metallic behavior down to low temperatures have not been reported for SWNTs (*12*). Our observation of these phenomena may be the result of the good metallic contacts of our samples. Moreover, intrinsic electronic transport properties of SWNTs are more likely to be observed in suspended nanotubes than in deposited tubes, where they could be altered by the substrate. Metallic behavior is also observed for single SWNTs where $R_0 < 30$ kilohms.

In the rope samples mounted on Re/Au contacts consisting of bilayers (30-nm layer of Re; 50-nm layer of Au) with a transition temperature $T_c = 1.1$ K (Fig. 2), the resistance became temperature dependent below 1.5 K in the region of the superconducting transition of the Re/Au contact. For the highest resistivity sample $R0_1$ ($R_0 = 1750$ ohms),

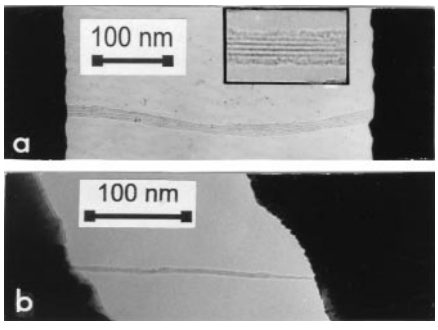

Fig. 1. Transmission electron micrograph of the nanotubes, suspended across a slit between two metallic pads. From these micrographs, it is possible to confirm that the metal of the contacts neither covers nor penetrates the tubes. (**a**) Nanotube ropes. The measured length L and diameter D of the samples studied were: $R0_1$ and $R0_2$: $L = 0.5$ μm, $D = 20$ nm; $R0_3$: $L = 1.7$ μm, $D = 23$ nm. (**b**) Sample ST_1 consists of a single SWNT of 0.3 μm length, which is completely isolated at one end for a length of 50 nm, but merges into a narrow rope of seven tubes (0.2 μm length) on the other end.

[1]Laboratoire de Physique des Solides, Associé au CNRS, Bâtiment 510, Université Paris-Sud, 91405, Orsay, France. [2]Institute of Microelectronics Technology and High Purity Materials, Russian Academy of Sciences, Chernogolovka 142432 Moscow Region, Russia. [3]Groupe de Dynamique des Phases Condensées, Université Montpellier II, 34095 Montpellier, France. [4]Max-Planck-Institute, D-70506 Stuttgart, Germany.

*To whom correspondence should be addressed. E-mail: bouchiat@lps.u-psud.fr

only a small dip was observed and the resistance increased at low temperature. For sample $R0_2$ (R_0 = 650 ohms), the resistance decreased linearly with temperature below 1 K and extrapolated to zero at 0 K. Samples $R0_1$ and $R0_2$ are too resistive and do not fulfill the condition $L_T > L$ necessary to achieve superconductivity. In contrast, the resistance of the rope $R0_3$, which contains approximately 200 tubes, is R_0 = 65 ohms; the average resistance for each tube is on the order of 13 kilohms, only a factor of 2 larger than that expected for a pure metallic tube. This sample underwent a superconducting transition and exhibited zero resistance below 1 K. Taking the Fermi velocity $v_F = 0.8 \times 10^6$ m s^{-1}, we estimate for this sample L_T (T = 1 K) on the order of 3 μm, larger than its length of 1.7 μm. We also observed proximity-induced superconductivity in isolated SWNT samples like ST_1 (Fig. 1), with R_0 = 27 kilohms. This value is on the order of the inverse quantum conductance h/e^2 = 25.8 kilohms, the maximum value for which low temperature metallic behavior is expected in a coherent one-dimensional system. The tube was mounted on Ta/Au electrodes (5-nm Ta, 100-nm Au) and had a superconducting transition at T_c = 0.4 K, close to the transition temperature of the contacts. The transition was shifted to lower temperature when a magnetic field was applied in the plane of the contacts (perpendicular to the tube axis). The critical field was surprisingly high (of the order of 1 T) and was 10 times larger than the measured critical field of the contact. Above 2 T, the resistance became field-independent and a small increase was apparent when the temperature was lowered below 0.2 K (Fig. 2B). Similar behavior was observed in $R0_3$ and all the nanotube junctions which exhibit superconductivity.

The most striking signature of induced superconductivity is the existence of Josephson supercurrents through the samples $R0_3$ and ST_1. The results of nonlinear transport measurements performed on these superconducting samples are exemplified by the voltage versus current characteristics on sample ST_1 (Fig. 3). The transition between the superconducting state (zero voltage drop through the sample) and the dissipative state is quite abrupt and displays hysteresis at low temperature. It is characterized by a critical current i_c whose value at $T \approx 0$ K is i_0 = 2.5 μA for $R0_3$ and i_0 = 0.104 μA for ST_1. We note that the junction does not recover its normal resistance above the critical current, and the curve $V(I)$ exhibits subsequent hysteretic jumps at higher currents.

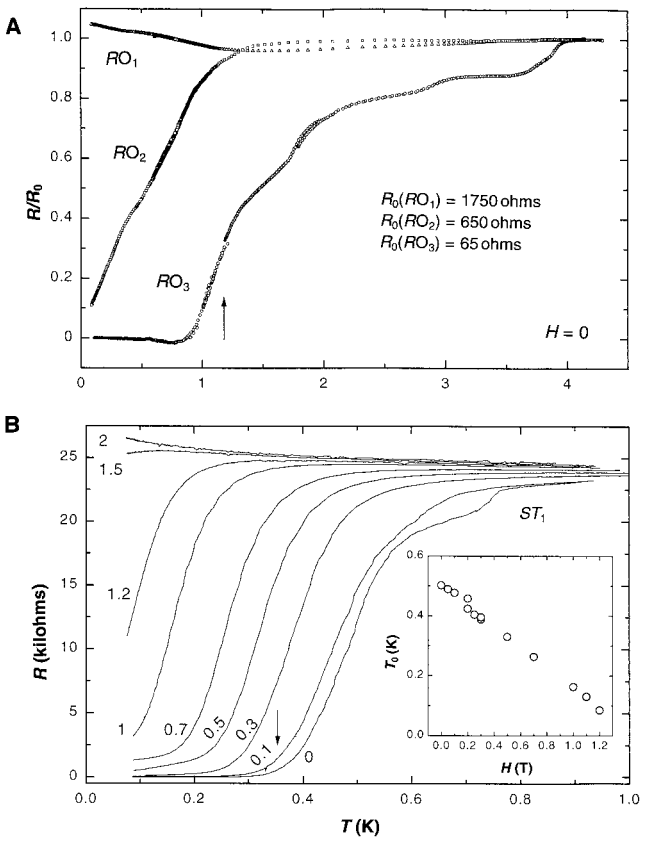

Fig. 2. (**A**) Temperature dependence of the resistance of ropes $R0_1$, $R0_2$, and $R0_3$ mounted on Au/Re contacts measured for zero magnetic field. The arrow indicates the transition of the Au/Re bilayer. The sample $R0_3$ becomes superconducting below 1 K, but the existence of resistance steps above the transition indicates that superconductivity may not be homogeneous. (**B**) Temperature dependence of the resistance of the single tube ST_1 mounted on Au/Ta measured for different values of the magnetic field perpendicular to the tube axis. (The labels on the curves correspond to the value of magnetic field in Tesla.) The arrow indicates the transition temperature of the contact in zero magnetic field. (Inset) Field dependence of the transition temperature [defined as the inflexion point of $R(T)$].

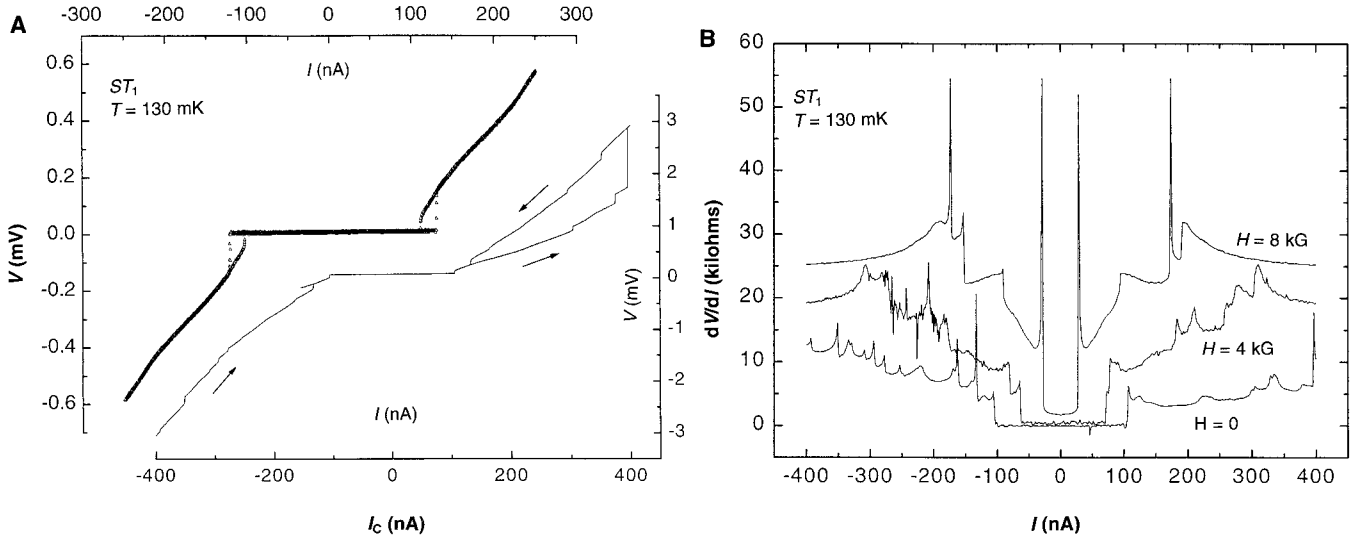

Fig. 3. (**A**) (Upper curve) $V(I)$ characteristics for ST_1, from which the critical current is deduced. (Lower curve) The same data on a wider current scale showing the existence of voltage steps for currents higher than i_c. (**B**) Differential resistance measured with a small ac modulation of the current for various values of the magnetic field. This data indicates that the normal resistance R_N = 25 kilohms is only recovered at currents much higher than i_c.

This behavior is similar to that observed in long superconducting filaments (*14*), where above i_c, small normal regions (of size comparable to the inelastic length) appear located around defects in the sample (phase-slip centers). However, the precise understanding of the physical mechanism involved in an SWNT with similar aspect ratio, but with dimensions 100 times smaller, requires further experimental and theoretical study.

The critical current decreases with temperature and goes to zero at $T \approx T_c$ (Fig. 4). This temperature dependence is very different for $R0_3$ and ST_1 samples. For $R0_3$, $i_c(T)$ is nearly flat below 0.5 K and decreases rapidly at higher temperature. This behavior approximately follows the classical Ambegaokar-Baratoff expression for Josephson tunnel junctions, $i_{AB}(T)$. This fit is valid in the limit where $L \ll L_T$; deviations to this fit are observed in the vicinity of T_c where this relation is no longer valid (Fig. 4). [Note that the weak link junction results of Kulik-Omelianchuck (*7*) do not fit our data at all.] The theoretical value $i_0 = (\pi/2)(\Delta/eR_N)$ corresponds to 3.8 μA, which is larger than but of the same order of magnitude as the experimental value [we assumed that the Bardeen-Cooper-Schrieffer (BCS) relation $\Delta = 1.76k_BT_c$ is fulfilled for the contact]. The behavior of the single tube ST_1 is more surprising. The value of the product R_Ni_c at $T = 0$ is equal to 2.5 mV, 40 times larger than the expected value (0.06 mV) assuming the gap is identical to its value in the superconducting electrodes (as estimated from T_c). The temperature dependence of the critical current is very weak below 0.8 T_c and does not follow the BCS gap temperature dependence. On the other hand, the critical current decreases linearly with the magnetic field and goes to zero at $H_c = 1$ T, coinciding with the value of H_c determined by linear transport experiments.

An explanation of these phenomena is not straightforward. The problem of an SNS junction constituted of a Luttinger liquid between two superconducting reservoirs has been considered theoretically by Fazio *et al.* (*15*) for weakly transmitting contacts and Maslov *et al.* (*16*) for perfectly transmitting contacts. In both cases, these authors show that it is indeed possible to induce superconductivity by a proximity effect. In the case of repulsive interactions and perfectly transmitting interfaces, the zero temperature value of the critical current is not changed by the interactions. This result could be modified by the presence of disorder in the system and needs further investigation. The calculated temperature dependence of the critical current is weaker than for noninteracting electrons. At this stage, it is clear that these results do not explain our data on ST_1. However, it has also been shown that coupling with low energy phonons can turn repulsive interactions in a Luttinger liquid into attractive ones and drive the system toward a superconducting phase (*17*). In our case, from the frequency of the fundamental bending mode of the suspended tubes, we can estimate that the characteristic energy scale of such phonons is in the range of 0.2 to 0.4 K.

Our data could indeed be explained by the existence of superconducting fluctuations intrinsic to SWNTs. For an infinite nanotube, because of its one-dimensional character, these fluctuations are not expected to give rise to a superconducting state at finite temperature. However, the superconducting state might be stabilized by the macroscopic superconductivity of the contacts. In such a situation, it is conceivable to expect that i_c could be enhanced compared to its value in a conventional SNS junction. The existence of superconducting fluctuations intrinsic to nanotubes may also explain the positive magnetoresistance (*18*) observed in all our samples where the normal state resistance is recovered at fields much higher than the critical field of the contacts.

Carbon nanotubes suspended between superconducting contacts constitute a new type of Josephson junction that offers a number of exciting possibilities. For example, because of their low electronic density, one may hope to be able to tune the superconducting properties with a metallic gate located close to the tube. Their suspended character also offers the possibility of interesting bolometric applications.

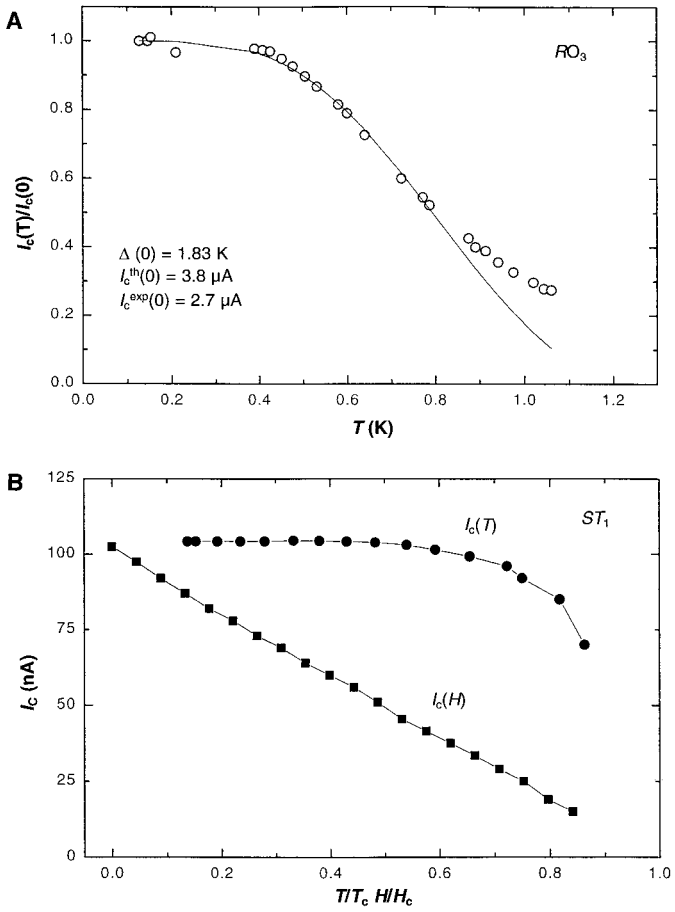

Fig. 4. (**A**) Temperature dependence of the critical current measured in the rope $R0_3$ (circles) fitted with the Ambegaokar-Baratoff formula $i_{AB}(T) = i_0 \frac{\Delta(T)}{\Delta(0)} \tanh[\Delta(T)/2k_BT]$ (continuous line). (**B**) Temperature and magnetic field dependence of the critical current of the superconducting single tube ST_1. The critical current disappears at $H_c = 1$ T. This value is identical with the estimation of the low-temperature critical field from the $R(T)$ curves in Fig. 2B.

References and Notes

1. M. S. Dresselhaus, G. Dresselhaus, P. C. Eklund, *Science of Fullerenes and Carbon Nanotubes* (Academic Press, San Diego, CA, 1996).
2. C. Kane, L. Balents, M. P. Fisher, *Phys. Rev. Lett.* **79**, 1932 (1997).
3. S. T. Tans *et al.*, *Nature* **394**, 761 (1998).
4. G. Deutscher and P. G. de Gennes, in *Superconductivity*, R. D. Parks, Ed. (Dekker, New York, 1969), pp. 1005–1033.
5. R. B. van Dover, A. de Lozanne, M. R. Beasley, *J. Appl. Phys.* **52**, 7327 (1981).
6. H. Courtois, Ph. Gandit, B. Panetier, *Phys. Rev. B* **52**, 1162 (1995).
7. For a review of supercurrents through superconducting junctions, see K. Likharev [*Rev. Mod. Phys.* **51**, 101 (1979)].
8. C. Journet *et al.*, *Nature* **388**, 756 (1997).
9. M. Burghard *et al.*, in *Electronic Properties of Novel Materials*, H. Kuzmany *et al.*, Eds. (American Institute of Physics, New York, 1998), pp. 44–49.
10. A focused laser beam released a nanotube from a target onto the sample with a Si_3N_4 membrane coated with a metal film. A submicrometer-width slit about 100 μm in length had previously been cut in the membrane with a focused ion beam; the nanotube connected the edges of the slit and shorted the electric circuit, whose resistance was >1 gigohm before the nanotube was "shaken off."
11. A. Yu. Kasumov, I. I. Khodos, P. M. Ajayan, C. Colliex, *Europhys. Lett.* **34**, 429 (1996); A. Yu. Kasumov *et al.*, *ibid.* **43**, 89 (1998).
12. M. Bockrath *et al.*, *Science* **275**, 1922 (1997); J. E. Fisher *et al.*, *Phys. Rev. B* **55**, 4921 (1997).

13. P. Delaney *et al.*, *Nature* **391**, 466 (1998).
14. J. Meyer and G. Minnigerode, *Phys. Lett. A* **38**, 529 (1972).
15. R. Fazio, F. W. J Hekking, A. A. Odintsov, *Phys. Rev. B* **53**, 6653 (1996).
16. D. L. Maslov, M. Stone, P. M. Goldbart, D. Loss, *ibid.*, p. 1548.
17. D. Loss and T. Martin, *ibid.* **50**, 12160 (1994).
18. A. Yu. Kasumov *et al.*, unpublished data.
19. We acknowledge A. Loiseau for collaboration with the preparation of SWNTs on TEM grids and A. MacFarlane for useful comments on the manuscript. We also benefited from fruitful discussions with M. Dévoret, D. Estève, C. Urbina, T. Giamarchi, H. Pothier, and H. Raffy. A.K. thanks The Russian Foundations for Basic Research (grant no. 97-1061) and Solid-State Nanostructures (99-02-1061) for financial support.

31 December 1998; accepted 26 April 1999

A Post-Stishovite SiO_2 Polymorph in the Meteorite Shergotty: Implications for Impact Events

T. G. Sharp,[1]* A. El Goresy,[2]† B. Wopenka,[3] M. Chen[4]

Transmission electron microscopy and electron diffraction show that the martian meteorite Shergotty, a shocked achondrite, contains a dense orthorhombic SiO_2 phase similar to post-stishovite SiO_2 with the α-PbO_2 structure. If an SiO_2 mineral exists in Earth's lower mantle, it would probably occur in a post-stishovite SiO_2 structure. The presence of such a high-density polymorph in a shocked sample indicates that post-stishovite SiO_2 structures may be used as indicators of extreme shock pressures.

The SiO_2 polymorph stishovite forms at high pressure (*1*), and has been found in highly shocked rocks (*2*). The existence and stability of post-stishovite silica (SiO_2 polymorphs denser than stishovite) have been the subject of many recent studies (*3*–*14*). Post-stishovite silica plus magnesiowüstite might be stable relative to (Mg,Fe)SiO_3-perovskite in Earth's lower mantle (*13*, *15*–*17*). Such an SiO_2 phase in heavily shocked samples would also provide a tool for understanding impact processes. Here we describe a post-stishovite SiO_2 phase in the martian meteorite Shergotty.

Shergotty is heavily shocked; it contains maskelynite (*18*–*20*), which was long thought to be diaplectic plagioclase glass that formed by a solid-state transformation (*21*), but appears to have quenched from a shock-induced melt (*22*). Shergotty also contains large silica grains (>150 mm) that were previously interpreted to be birefringent shocked quartz with planar deformation features (*21*). Most are wedge-shaped, which is typical of β-tridymite but atypical of quartz. Like many of the maskelynite grains (*22*), the silica grains lack shock-induced intragranular fractures. Many of the SiO_2 grains are surrounded by radiating cracks (Fig. 1A). These cracks are similar to those formed around coesite in high-pressure metamorphic rocks (*23*) and indicate that the volume of the silica phase increased greatly with decompression. Expansion must have occurred when the maskelynite was solid, because the cracks also cut through it (Fig. 1B). The lamellar texture appears as two sets of lamellae of different brightness in field-emission scanning electron microscopy images recorded in back-scattered-electron (BSE) mode (Fig. 1B). Electron microprobe (EMP) analyses of the largest lamellae (up to several micrometers wide), using a slightly defocused electron beam, revealed that both the bright and dark lamellae are SiO_2 compounds that are identical in composition and have minor concentrations of Na_2O (0.4% by weight) and Al_2O_3 (1.12%). BSE imaging with a field-emission scanning electron microscope (FESEM) at low accelerating voltages revealed that the original silica grains consist of a mosaic of many individual domains (10 to 50 μm in diameter), each with a distinct pattern of intersecting thin (<300 nm) lamellae (Fig. 1B).

We investigated the crystallinity and structure of SiO_2 phases using laser Raman microprobe spectroscopy, transmission electron microscopy (TEM), and selected-area electron diffraction (SAED). Three zone-axis SAED patterns (Fig. 2) were collected from a domain of crystalline material. These patterns all show sharp intensity maxima and diffuse rings, corresponding to diffraction from the crystalline material and diffuse scattering from amorphous material, respectively. Starting from zone axis 1 (Fig. 2A), the crystal was tilted 21° about the vertical diffraction vector (with d spacing = 4.54 Å) to reach zone axis 2 (Fig. 2B). The reflection corresponding to 4.54 Å disappeared as the sample was tilted out of zone axis 1 and remained absent in zone axis 2, indicating that it is a forbidden reflection that occurs by dynamical diffraction in zone axis 1. Zone axis 3 (Fig. 2C) was reached by tilting the crystal 37° from zone axis 1 about the horizontal diffraction vector (d = 3.22 Å). In this case, the d = 3.22 Å reflection remained excited and therefore is not forbidden. The three zone axis patterns contain seven diffraction vectors that can be used to constrain the structure of this SiO_2 polymorph.

The diffraction data (Fig. 2) cannot be indexed using the structures of SiO_2 polymorphs that are stable at low pressures. Although tridymite is a likely SiO_2 phase in Shergotty before shock metamorphism, the diffraction data are inconsistent with all tridymite polymorphs (*24*). Similarly, the diffraction data are inconsistent with coesite and stishovite. The data are also inconsistent with known post-stishovite structures, including the $CaCl_2$, baddelyite, and α-PbO_2, and modified baddelyite (*Pnc*2) structures of SiO_2. The diffraction data from zone axis 1 fit a post-stishovite structure with space group *Pbcn* that is similar to the α-PbO_2 structure (*25*-*27*), but the d spacings from zone axes 2 and 3 fit less well to this α-PbO_2–like structure (*27*). Our data also nearly fit a $Pca2_1$ structure calculated to be a quench phase from post-stishovite SiO_2 at 50 GPa and a 10-GPa differential stress (*28*). The cell parameters of $Pca2_1$ and *Pbcn* structures are nearly the same, but they do not match the 1.97 Å and 3.41 Å d spacings of our data (Table 1).

Because the symmetries of our diffraction patterns are consistent with an orthorhombic lattice and the reflections can be indexed to *Pbcn* and $Pca2_1$ structures (*27*, *28*), we refined new orthorhombic cell parameters to fit our data (Table 1). All our d-space data fit the refined orthorhombic unit cells within 1% (Ta-

Table 1. d-space data obtained from the three zone-axis diffraction patterns as compared to calculated d spacings for *Pbcn* and $Pca2_1$ SiO_2 structures (*27*, *28*) and the refined unit cells based on the *Pbcn* structure. Miller indices (*hkl*) are also given for each structure, with an asterisk indicating the reflections that are forbidden

SAED	*Pbcn*		$Pca2_1$		Refined *Pbcn*	
4.54*	001*	4.50	100*	4.49	001*	4.55
3.41	011*	3.25	110	3.25	011*	3.40
3.22	110	3.17	011*	3.17	110	3.23
3.09	101*	3.11	101*	3.11	101*	3.07
2.62	111	2.59	111	2.59	111	2.63
2.28	002	2.25	200	2.25	002	2.28
1.97	121	1.88	121	1.88	121	1.97

[1]Department of Geology, Arizona State University, Tempe, AZ 85287, USA. [2]Max-Planck-Institut für Kernphysik, Post Office Box 103 980, 69029 Heidelberg, Germany. [3]Department of Earth and Planetary Sciences, Washington University, St. Louis, MO 63130, USA. [4]Guangzhou Institute of Geochemistry, Academie Sinica, Guangzhou 510640, China.

*To whom correspondence should be addressed.
†Present address: Max-Planck-Institut für Chemie, J.-Becher-Weg 27, 55128 Mainz, Germany.